A novel hyperchaotic map with sine chaotification and discrete memristor

Qiankun Sun(孙乾坤), Shaobo He(贺少波), Kehui Sun(孙克辉)†, and Huihai Wang(王会海)

School of Physics and Electronics, Central South University, Changsha 410083, *China*

(Received 28 July 2022; revised manuscript received 30 August 2022; accepted manuscript online 5 September 2022)

Discrete memristor has become a hotspot since it was proposed recently. However, the design of chaotic maps based on discrete memristor is in its early research stage. In this paper, a memristive seed chaotic map is proposed by combining a quadratic discrete memristor with the sine function. Furthermore, by applying the chaotification method, we obtain a high-dimensional chaotic map. Numerical analysis shows that it can generate hyperchaos. With the increase of cascade times, the generated map has more positive Lyapunov exponents and larger hyperchaotic range. The National Institute of Standards and Technology (NIST) test results show that the chaotic pseudo-random sequence generated by cascading two seed maps has good unpredictability, and it indicates the potential in practical application.

Keywords: discrete memristor, hyperchaotic map, cascade, pseudo-random number generator

PACS: 05.45.–a, 05.45.Jn, 05.45.Pq **DOI:** 10.1088/1674-1056/ac8f3a

1. Introduction

Memristor was proposed by Professor Chua in 1971 according to the completeness of circuit theory.[1] It represents the relationship between charge and magnetic flux. Later, Professor Chua put forward the concept of generalized memristor.[2] However, since it only stayed at the theoretical level at that time, the memristor had not made much progress. Until 2008, HP laboratory firstly reported the real memristor device,[3] which ignited an upsurge of research. Memristor is a nonlinear element with internal state that is completely different from the traditional circuit element, and it can be used to construct circuits with complex chaotic oscillations.[4] Moreover, memristor attracted extensive attention in the scientific community, and was applied in nanotechnology,[5,6] electrical engineering,[7,8] neural network,[9,10] image processing,[11,12] and so on.

It should be noticed that most studies on memristive chaotic systems are limited to the continuous-time domain.[13–17] Comparing with continues memristor, the discrete memristor is more suitable for digital circuits and discrete chaotic maps, which is easily implemented by hardware circuits, and the discrete chaotic maps avoid the disadvantage that the results are difficult to repeat due to the sensitivity of chaos. The design of discrete memristive chaotic maps is a new topic. He *et al.* designed an integer-order discrete memristor model and introduced it into several typical chaotic maps.[18,19] Meanwhile, a fractional-order discrete memristor was proposed based on the fractional difference theory and it was added to the Sine function.[20] In 2022, Zhu *et al*. reviewed the existing memristive elements, including integer-order and fractional-order memristive systems, and analyzed their similarities and differences.[21] Bao *et al*. reported a new second-order discrete memristive hyperchaotic map.[22] Wang *et al*. constructed a memristor model and used it to simulate a synaptic connection in a Hopfield neural network.[23] In 2021, Fu *et al*. established the Simulink model of discrete memristive chaotic map and furtherly verified the feasibility of discrete memristor.[24] In addition, many interesting phenomena, such as coexisting attractors,[25–27] hidden attractors,[28] and multistability,[29] were discovered in memristive chaotic maps and the chaotic maps were used in secure communication successfully.[30,31]

Over the past few years, many people were devoted to the work of enhancing chaos. Hua *et al*. designed several new chaotic maps by cascading and coupling methods.[32–34] Theoretical verification and experimental results showed that the Lyapunov exponent and chaotic interval were much larger than that of subsystems. Moreover, Hua *et al*. obtained a high-dimensional Cat map by using a one-dimensional Cat map.[35] Zheng *et al*. studied chaos by adding a state feedback controller.[36] Yuan *et al*. designed a cascade memristive chaotic map,[37] but they did not make the internal variables store in the system, and with the increase of cascade times, the total dimension of the generated map did not increase. Inspired by the above discussions, we focus on designing high-dimensional hyperchaotic maps by using the discrete memristor. The rest of this paper is arranged as follows. In Section 2, the quadratic discrete memristor and the memristive chaotic map is presented. In Section 3, the chaotification method and the higher dimensional hyperchaotic map are de-

†Corresponding author. E-mail: kehui@csu.edu.cn

© 2022 Chinese Physical Society and IOP Publishing Ltd

signed. In Section 4, the dynamical behaviors are analyzed. In Section 5, the NIST test is presented. Finally, we summarize this paper and indicate the future work.

2. The quadratic memristive hyperchaotic map

2.1. The quadratic discrete memristor

According to the definition of continuous-time memristor, the charge controlled memristor is defined by[35]

$$\begin{cases} v(t) = M(q(t))i(t), \\ \dfrac{\mathrm{d}q(t)}{\mathrm{d}t} = i(t), \end{cases} \tag{1}$$

where $v(t)$ and $i(t)$ are the voltage and the current respectively. $M(q(t))$ represents the resistance function, and $q(t)$ is the amount of charge. The relationship between $q(t)$ and $i(t)$ is defined by

$$q(t) = \int_{-\infty}^{t} i(t)\,\mathrm{d}t. \tag{2}$$

By introducing the difference theory, the discrete memristor is designed as

$$\begin{cases} v_n = M(q_n)\, i_n, \\ q_{n+1} = k i_n + q_n, \end{cases} \tag{3}$$

where v_n and q_n represent the values of $v(t)$ and $q(t)$ at the n-th iteration, and the equation $q_{n+1} = q_n + k i_n$ is deduced as

$$\begin{aligned} q_2 &= q_1 + k i_1, \\ q_3 &= q_2 + k i_2, \\ &\cdots, \\ q_n &= q_{n-1} + k i_{n-1}. \end{aligned} \tag{4}$$

Therefore, q_n is written as

$$q_n = q_1 + k \sum_{j=1}^{n-1} i_j, \tag{5}$$

and equation (1) becomes to

$$v_n = M\left(q_1 + k \sum_{j=1}^{n-1} i_j\right) i_n. \tag{6}$$

Thus, it demonstrates that the current state of the discrete memristor depends on all of the past states. Here, we choose $M(q_n)$ as the quadratic function $q_n^2 - 1$, and equation (3) becomes to

$$\begin{cases} v_n = \left(q_n^2 - 1\right) i_n, \\ q_{n+1} = q_n + k i_n, \end{cases} \tag{7}$$

where k is the internal control parameter. Here, we set $k = 0.8$.

To verify whether the memristor satisfies the definition of a memristor, we add a sinusoidal voltage signal $I_n = A\sin(\omega n)$ to it. The changes of the voltage and the current sequences are shown in Fig. 1(a). The phase diagrams of v_n–i_n with the variation of A, ω, and the initial value m_0 are shown in Figs. 1(b), 1(c), and 1(d) respectively. It indicates that this discrete memristor meets the three fingerprints of a generalized memristor.[39]

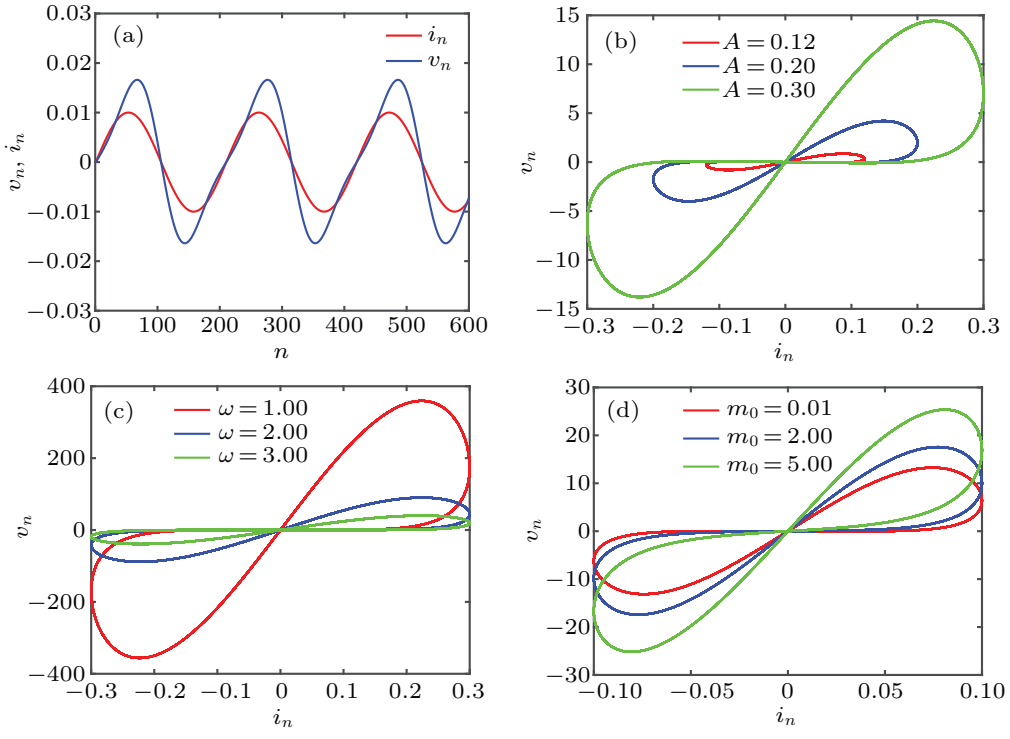


Fig. 1. The sequences of v_n, i_n, and the three fingerprints of the memristor: (a) the sequences of v_n, i_n, $A = 0.01$, $\omega = 3$, $m_0 = 1.3$ and the three fingerprints of the memristor when (b) $\omega = 5$, $m_0 = 0.01$, $A = 0.12$, 0.2, 0.3, and (c) $A = 0.3$, $m_0 = 0.01$, $\omega = 1$, 2, 3 and (d) $\omega = 1$, $A = 0.1$, $m_0 = 0.01$, 2, 5.

2.2. The quadratic memristive chaotic map

In the discrete memristor, denote i_n as the input for the n-th iteration and v_n as the output and the next input of the iteration. The quadratic memristive chaotic map (QMCM)[40] is presented as

$$\begin{cases} x_{n+1} = \mu\left(y_n^2 - 1\right)x_n, \\ y_{n+1} = kx_n + y_n, \end{cases} \tag{8}$$

where μ and k are the control parameters. x_{n+1} is the output variable, and y_{n+1} is the internal state variable. The block diagram of QMCM is presented in Fig. 2(a). When the parameters are set as $\mu = 1.76$, $k = 0.8$ with the initial values $(x_1, y_1) = (-0.5, 0.3)$, the maximum Lyapunov exponent (MLE) is 0.2384, which indicates it is in the chaotic state. The attractor is plotted in Fig. 2(b).

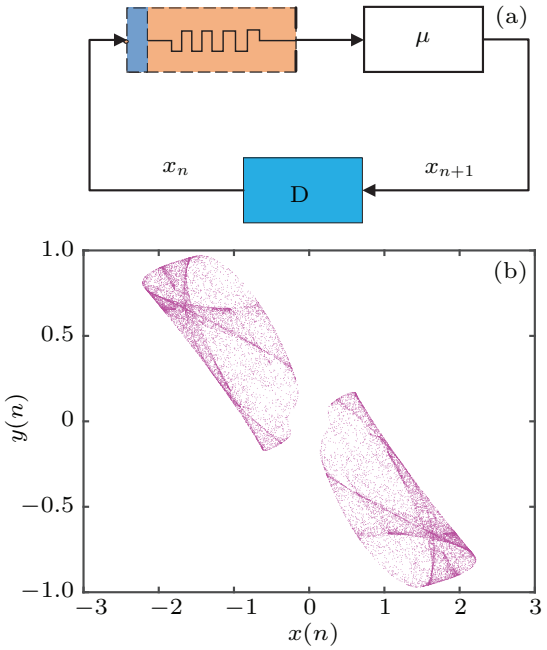


Fig. 2. The block diagram and the attractor of QMCM. (a) The block diagram and (b) the attractor when $\mu = 1.76$, $k = 0.8$.

3. The cascaded memristive hyperchaotic map

3.1. The chaotification methods

Sine chaotification method (SCM) has been proven to be effective in expanding the chaotic range and increasing the chaotic complexity.[34,41] The principle of SCM is to transform the output of a chaotic map with the sine function, and the mathematical equation of SCM is expressed as

$$x_{n+1} = \mathbb{S}(x_n) = \sin\left(\lambda F(x_n)\right), \tag{9}$$

where λ is the control parameter.

Cascade chaotification method (CCM) which connects two chaotic maps in series is shown to make the chaotic map be more unpredictable and have larger parameter interval. The output of $G(x)$ is used as the input of $F(x)$. The mathematical expression is

$$x_{n+1} = F \circ G(x_n) = F(G(x_n)). \tag{10}$$

Finally, we delay the output of the previous seed map x_{n+1} to get x_n, and then take x_n as the input of the next seed map. The state variable y_{n+1} is stored in the memristor. It is worth mentioning that the functions of the resistance can be the same or different to generate different maps.

According to SCM, we take x_{n+1} in Eq. (8) as the input of the sine function, and get the sine-quadratic memristive hyperchaotic map (S-QMHM). Thus, the seed map is expressed as

$$\begin{cases} x_{n+1} = \varepsilon \sin\left(\mu\left(y_n^2 - 1\right)x_n\right), \\ y_{n+1} = kx_n + y_n, \end{cases} \tag{11}$$

where ε and μ are the external control parameters, and k is the internal control parameter. We set them to $\mu = 1.78$, $k = 0.8$, and get the attractors with different ε, which is shown in Fig. 3. When $\varepsilon = 2.1131$, the MLE is -0.2338, and the map exhibits a periodic state. As $\varepsilon = 2.3755$, the map has one positive Lyapunov exponent equal to 0.3014, which means it is in the chaotic state, and it is in the hyperchaotic state when $\varepsilon = 2.2801$ with two positive Lyapunov exponents.

The structure of the cascaded S-QMHM is presented in Fig. 4. For the i-th iteration, $x_i(0)$ is input into DM_1, and then goes through the sine function and the delay unit to get $x_i(1)$. The obtained sequence $x_i(1)$ is used as the input of the second memristor DM_2, and then goes through the sine function and the delay unit to get $x_i(2)$. In the same way, we finally get $x_i(m)$. So far, a complete iteration is completed. In the next iteration, $x_i(m)$ will be used as the initial value $x_{i+1}(0)$. Besides, $y_i(n)$ $(n = 1, 2, 3, \ldots, m)$ is stored in each memristor as an internal variable.

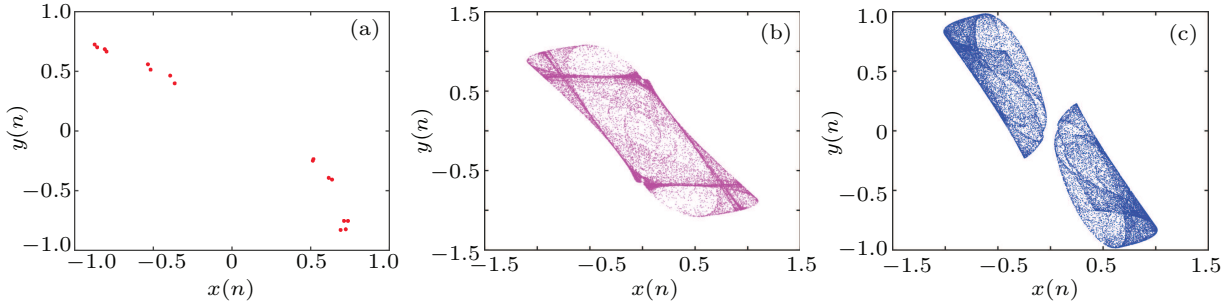


Fig. 3. Different attractors of S-QMHM: (a) $\varepsilon = 2.1131$, period; (b) $\varepsilon = 2.3755$, chaos; and (c) $\varepsilon = 2.2801$, hyperchaos.

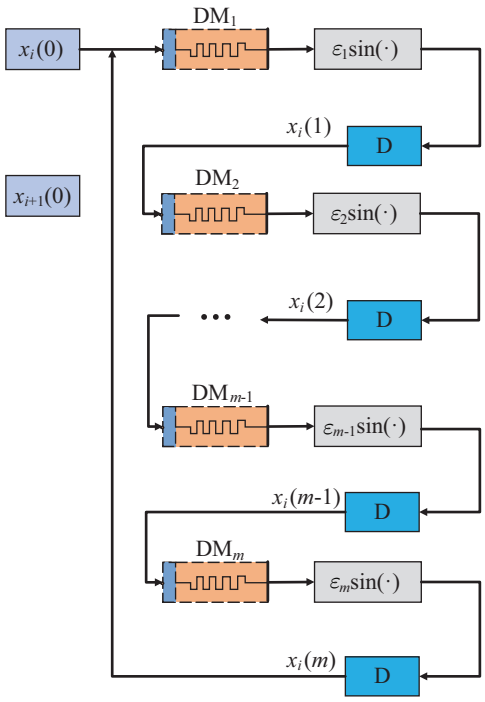


Fig. 4. The block diagram of the cascaded S-QMHM.

3.2. The higher dimensional hyperchaotic map

When m seed maps are cascaded, the mathematical model is defined by

$$\begin{aligned}
&x_1(n+1) = \varepsilon_1 \sin\left[\mu_1 M_1\left(y_1(n)\right) x_m(n)\right],\\
&x_2(n+1) = \varepsilon_2 \sin\left[\mu_2 M_2\left(y_2(n)\right) x_1(n)\right],\\
&x_3(n+1) = \varepsilon_3 \sin\left[\mu_3 M_3\left(y_3(n)\right) x_2(n)\right],\\
&\cdots,\\
&x_m(n+1) = \varepsilon_m \sin\left[\mu_m M_m\left(y_m(n)\right) x_{m-1}(n)\right],\\
&y_1(n+1) = k_1 x_m(n) + y_1(n),\\
&y_2(n+1) = k_2 x_1(n) + y_2(n),\\
&y_3(n+1) = k_3 x_2(n) + y_3(n),\\
&\cdots,\\
&y_m(n+1) = k_m x_{m-1}(n) + y_m(n),
\end{aligned} \tag{12}$$

where $\varepsilon_1, \varepsilon_2, \ldots, \varepsilon_m, \mu_1, \mu_2, \ldots, \mu_m$ are the output control parameters, and $k_1, k_2, \ldots, k_m$ are the internal control parameters. $M_i(y_i(n))$ depends on the different resistance functions of the memristor. It exhibits that the cascaded chaotic map with m seed maps can produce a $2m$-dimensional hyperchaotic map, which shows great potential of building high-dimensional hyperchaotic maps.

4. Dynamics analysis

4.1. Dynamics in the cascaded hyperchaotic map with two seed maps

4.1.1. The system model

Using the chaotification method proposed in Subsection 3.1 and the seed map in Subsection 3.2, we design the cascaded 2-sine-quadratic memristive hyperchaotic map (2-S-QMHM) which contains two seed maps. The mathematical model is

$$\begin{aligned}
x_1(n+1) &= \varepsilon_1 \sin\left[\mu_1\left(y_1^2(n)-1\right)x_2(n)\right],\\
x_2(n+1) &= \varepsilon_2 \sin\left[\mu_2\left(y_2^2(n)-1\right)x_1(n)\right],\\
y_1(n+1) &= k_1 x_2(n) + y_1(n),\\
y_2(n+1) &= k_2 x_1(n) + y_2(n),
\end{aligned} \tag{13}$$

and the block diagram is shown in Fig. 5.

We set the parameters to $\varepsilon_1 = 1.9$, $\varepsilon_2 = 2.28$, $\mu_1 = \mu_2 = 1.78$, $k_1 = k_2 = 0.8$, and the initial values $(x_1(1), x_2(1), y_1(1), y_2(1)) = (0.3, -0.1, 0.5, 0.2)$. The number of iteration n is set to 4×10^5, and the numerical results show that the MLE is 8.8272. The attractor is shown in Fig. 6, and it exhibits that the sequence has a wide distribution in three-dimensional space.

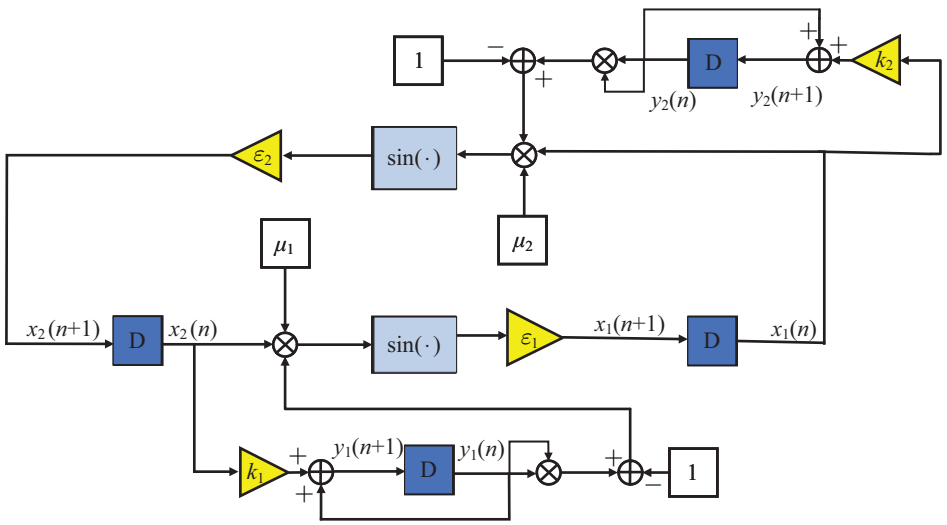


Fig. 5. The block diagram of 2-S-QMHM.

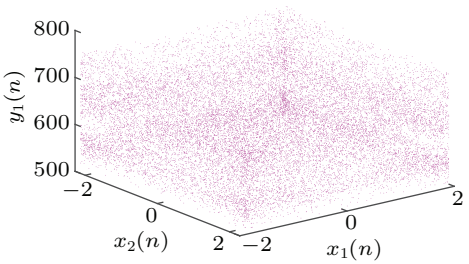


Fig. 6. The attractor of 2-S-QMHM.

4.1.2. Fixed point analysis

According to the Jacobian matrix and the fixed points expression $F=(0,y_i)$ of 2-S-QMHM ($i=1$, 2, and y_i is an arbitrary real constant). The characteristic matrix of 2-S-QMHM is

$$J=\begin{bmatrix} 0 & \varepsilon_1\mu_1\left(y_1^2-1\right) & 0 & 0 \\ \varepsilon_2\mu_2\left(y_2^2-1\right) & 0 & 0 & 0 \\ 0 & k_1 & 1 & 0 \\ k_2 & 0 & 0 & 1 \end{bmatrix}, \tag{14}$$

and its characteristic equation is deduced as

$$\begin{aligned}&(\lambda_1-1)(\lambda_2-1)\left(\lambda_3-\sqrt{\varepsilon_1\varepsilon_2\mu_1\mu_2\left(y_1^2-1\right)\left(y_2^2-1\right)}\right)\\ &\times\left(\lambda_4+\sqrt{\varepsilon_1\varepsilon_2\mu_1\mu_2\left(y_1^2-1\right)\left(y_2^2-1\right)}\right)=0.\end{aligned} \tag{15}$$

The eigenvalues are thereby calculated as $\lambda_1=1$, $\lambda_2=1$, $\lambda_3=(\varepsilon_1\varepsilon_2\mu_1\mu_2({y_1}^2-1)({y_2}^2-1))^{1/2}$, $\lambda_4=-\lambda_3$. Therefore, these eigenvalues are related to the parameters ε_1, ε_2, μ_1, μ_2 and the initial state y_1 and y_2. Since λ_1 and λ_2 always lie on the unit circle, the fixed point is critical stable when the absolute value of λ_3 and λ_4 are not greater than 1. Otherwise, the fixed point is unstable.

4.1.3. Lyapunov exponent and bifurcation

To show the dynamics of the proposed maps clearly, bifurcation diagram and Lyapunov exponents spectra (LEs) are used. We analyze the dynamical behaviors of the seed map and 2-S-QMHM. Noting that all LEs are iterated calculated 4×10^5 times.

When the initial values are set to $(x_0,y_0)=(0.3,0.5)$ and $k=0.8$, the LEs and bifurcation diagram of the seed map varying with ε, μ are shown in Fig. 7. It shows that when $\varepsilon\in(2.1,2.4)$ and $\mu\in(0.5,2.5)$, the map shows chaotic and hyperchaotic behavior. However, the length of the interval is small and there are many periodic windows. In practical applications, the value of the parameters that make the system appear periodic state should be avoided.

Similarly, the initial values of 2-S-QMHM are set to $(x_1(0),\ x_2(0),\ y_1(0),\ y_2(0))=(0.3,\ -0.1,\ 0.5,\ 0.2)$, and $k_1=k_2=0.8$. The LEs and bifurcation diagram varying with ε_1, μ_1 are shown in Fig. 8. At the range of (0, 5), there are three positive Lyapunov exponent within most of the interval, and two of them reach around 10. It is worth mentioning that the value of Lyapunov exponents still tends to become larger as the parameter increases. The other positive Lyapunov exponent oscillates around 0.01. Although the value is relatively small, it remains positive. Besides, the number of period window is reduced comparing to the seed map, making the system more stable.

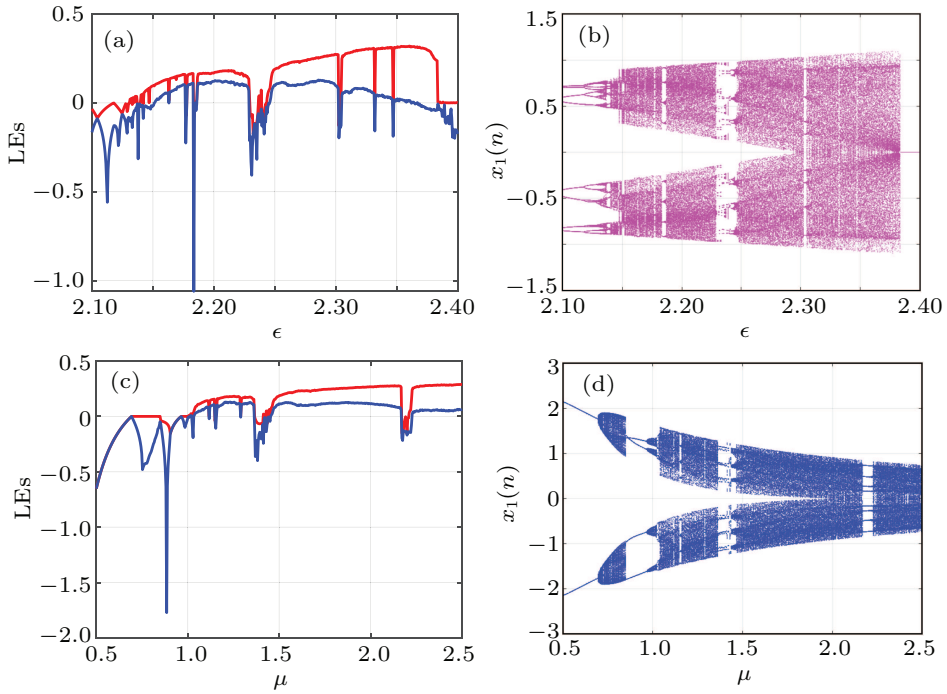


Fig. 7. LEs and bifurcation diagram of the seed map. When $\mu=1.78$, (a) LEs *versus* $\varepsilon\in(2.1,2.4)$, (b) bifurcation diagram *versus* $\varepsilon\in(2.1,2.4)$ and when $\varepsilon=2.28$, (c) LEs *versus* $\mu\in(0.5,2.5)$, (d) bifurcation diagram *versus* $\mu\in(0.5,2.5)$.

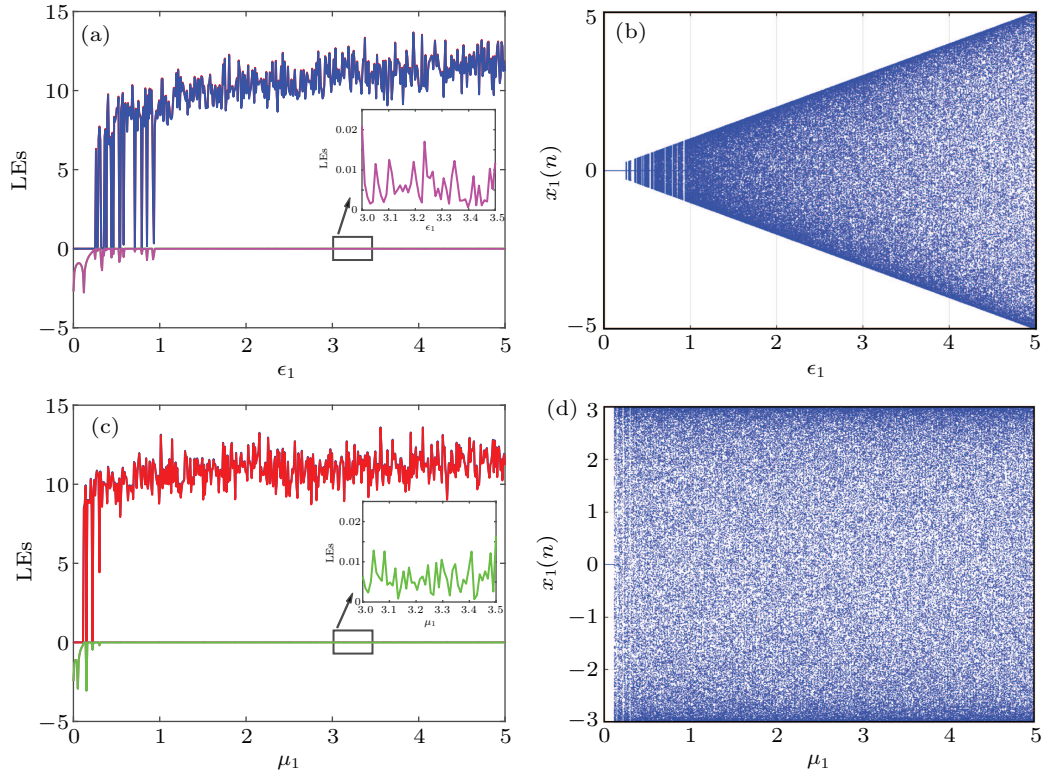


Fig. 8. LEs and bifurcation diagram of 2-S-QMHM. When $\varepsilon_2 = 2.9$, $\mu_1 = \mu_2 = 1.78$, (a) LEs *versus* $\varepsilon_1 \in (0, 5)$, (b) bifurcation diagram *versus* $\varepsilon_1 \in (0, 5)$ and when $\varepsilon_1 = 3$, $\varepsilon_2 = 2.28$, $\mu_2 = 1.78$, (c) LEs *versus* $\mu_1 \in (0, 5)$, (d) bifurcation diagram *versus* $\mu_1 \in (0, 5)$.

4.2. Dynamics in the higher-order cases

When 5 seed maps are cascaded, the LEs and bifurcation diagram varying with ε_1, μ_1 are shown in Fig. 9. Comparing with Fig. 8 for 2-S-QMHM, we see that 5-S-QMHM has more positive LEs and a larger hyperchaotic interval.

Table 1. the number of positive LEs and the MLE with cascade times.

No.	Number of seed maps	System dimension	Number of positive LEs	MLE
1	2	4	3	11.0029
2	3	6	5	11.2191
3	4	8	6	10.6321
4	5	10	8	10.6058
5	6	12	9	10.8198
6	7	14	11	10.6588
7	8	16	12	11.5119
8	9	18	14	11.3344
9	10	20	15	10.8953
10	11	22	17	11.2909

As analyzed above, a $2m$-dimensional chaotic map is generated by cascading m seed maps. We set the parameters here to be the same as the seed map. By the simulation experimental research, the cascaded hyperchaotic map has $m + [(m+1)/2]$ positive LEs ($[(m+1)/2]$ represents the largest integer no more than $(m+1)/2$). Among these LEs, m exponents oscillate around 10, and the remaining $[(m+1)/2]$ exponents keep positive despite their small values. Table 1 lists the number of positive Lyapunov exponent and the MLE with cascade times. Moreover, in the chaotic interval, changes in the parameters and the initial values do not affect the number of positive Lyapunov exponents.

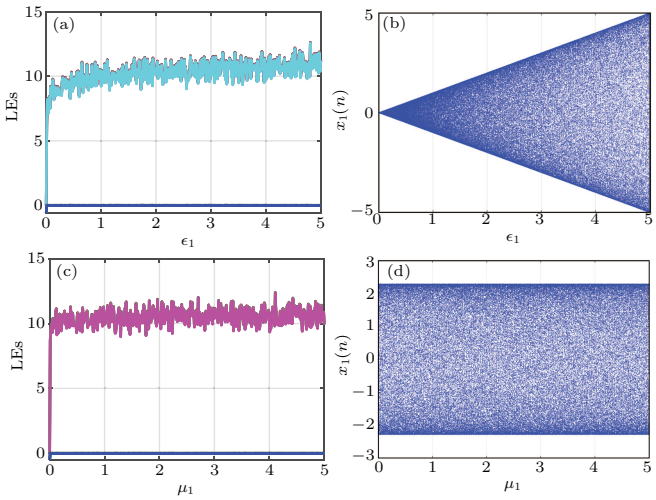


Fig. 9. LEs and bifurcation diagram of 5-S-QMHM. (a) LEs *versus* $\varepsilon_1 \in (0, 5)$ and (b) bifurcation diagram *versus* $\varepsilon_1 \in (0, 5)$ and (c) LEs *versus* $\mu_1 \in (0, 5)$ and (d) bifurcation diagram *versus* $\mu_1 \in (0, 5)$.

4.3. Sample entropy complexity analysis

Complexity is an indicator to measure the proximity of the chaotic sequence to the random sequence. The higher the complexity, the more random the chaotic sequence. We use the sample entropy algorithm to measure the complexity of these chaotic maps due to its high accurate in the statistical assessment of complexity.[42]

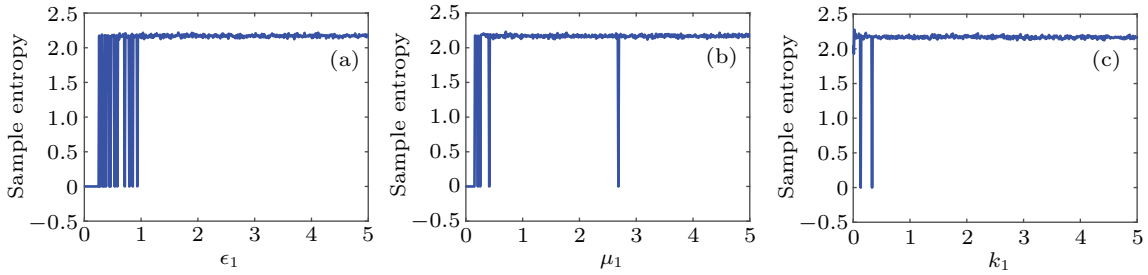


Fig. 10. Sample entropy of 2-S-QMHM with ε_1, μ_1, k_1: (a) $\varepsilon_2 = 2.9$, $\mu_1 = \mu_2 = 1.78$, $k_1 = k_2 = 0.8$, $\varepsilon_1 \in (0,5)$; (b) $\varepsilon_1 = 3$, $\varepsilon_2 = 2.28$, $\mu_2 = 1.78$, $k_1 = k_2 = 0.8$, $\mu_1 \in (0,5)$; and (c) $\varepsilon_1 = 3$, $\varepsilon_2 = 2.9$, $\mu_1 = \mu_2 = 1.78$, $k_2 = 0.8$, $k_1 \in (0,5)$.

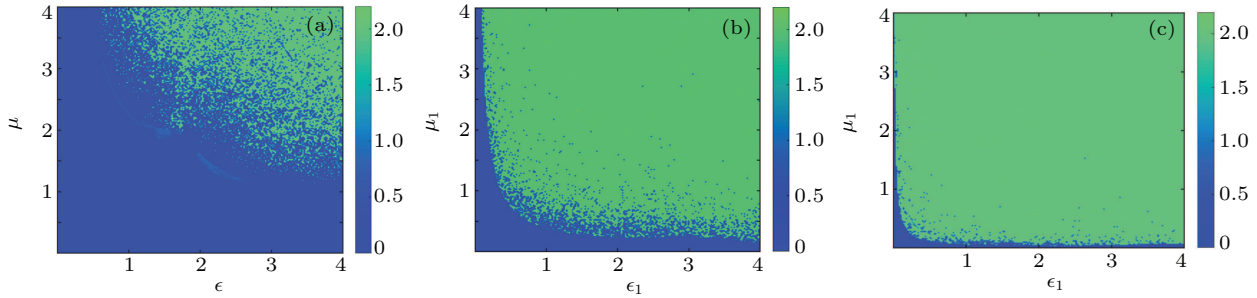


Fig. 11. Sample entropy of the seed map, 2-S-QMHM, and 3-S-QMHM: (a) the seed map (ε, μ) and (b) 2-S-QMHM (ε_1, μ_1), and (c) 3-S-QMHM (ε_1, μ_1).

In the following experiments, sample entropy of 2-S-QMHM is calculated *versus* ε, μ, and k. As it is shown in Fig. 10, sample entropy holds a small value in periodic windows and it remains greater than 2.2 in most range. In addition, the complexity of the seed map, 2-S-QMHM, and 3-S-QMHM are shown in Fig. 11, and it shows that the region with high complexity of the seed map is small. With the increase of cascade times, the high-complexity range gradually expands.

The sample entropy of the seed map, 2-S-QMHM, 3-S-QMHM, DM-based Hénon map,[18] DM-based cosine map,[43] and DM-based logistic map[33] are shown in Fig. 12. Obviously, 3-S-QMHM has larger sample entropy than that of other memristive chaotic maps.

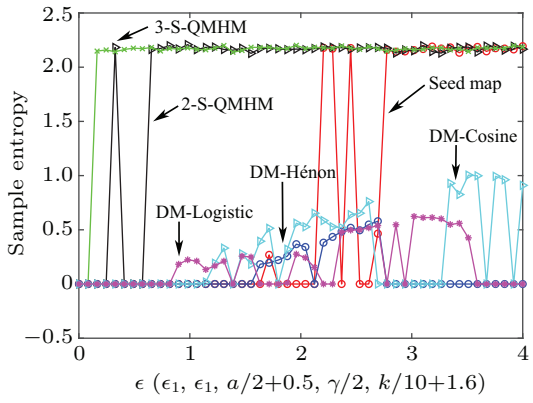


Fig. 12. Sample entropy of seed map(ε), 2-S-QMHM (ε_1), 3-S-QMHM (ε_1), DM-based Hénon map($a/2+0.5$), DM-based cosine map($\gamma/2$), and DM-based logistic map($k/2$).

5. Pseudo-random sequence generator

Pseudo-random sequence generator is one of the main applications of chaotic map. It is worth noting that the quantization algorithm is an important factor which affects the operation efficiency. For a chaotic sequence b generated by 2-S-QMHM, the quantization algorithm we adopt is described as follows:[44]

$$\begin{aligned}&\mathrm{PRBS}(8i:8(i+1)-1)\\&=\begin{cases}\mathrm{floor}\left(10^6\cdot x_i\right)\bmod 256, & x_i>0,\\ \mathrm{floor}\left(10^7\cdot x_i\right)\bmod 256, & x_i\leqslant 0.\end{cases}\end{aligned}\tag{16}$$

In this way, a sequence with a length of $8N$ is obtained after n iterations. In addition, two different quantization methods are adopted to switch, which increases the complexity and further improves the performance on the basis of little impact on the time efficiency.

As for 2-S-QMHM, we set the parameters to $\varepsilon_1 = 2$, $\varepsilon_2 = 2.28$, $\mu_1 = \mu_2 = 1.78$, $k_1 = k_2 = 0.8$, and the initial values $(x_1(0), x_2(0), y_1(0), y_2(0)) = (0.3, -0.1, 0.5, 0.2)$, then assess the randomness of the generated chaotic sequences by the NIST test. It includes 15 test indicators, and each indicator has two judgment bases, namely, pass rate and p-value. We set the significant level $\alpha = 0.01$, and number of test sequence group $\beta = 100$, and the length of each test sequence to 64. If the results meet the following two conditions at the same time, the sequences pass the NIST test.

(i) The pass rate of the test results is all within the confidence interval.

(ii) The p-value is greater than 0.0001.

In addition, the larger the p-value, the better the random performance. The test results are shown in Table 2. It shows that the sequences pass the NIST test successfully.

Table 2. NIST test result.

No.	Test index	Number of test[a]	p-value	Proportion	Result
1	frequency	1	0.13468	1.00	Pass
2	block frequency	1	0.97606	0.97	Pass
3	cumulative sums	2	0.31697	1.00	Pass
4	runs	1	0.77276	0.98	Pass
5	longest run	1	0.73991	1.00	Pass
6	rank	1	0.35048	1.00	Pass
7	FFT	1	0.80433	0.98	Pass
8	nonoverlapping template	148	0.42517	0.99	Pass
9	overlapping template	1	0.02818	1.00	Pass
10	universal	1	0.29925	0.99	Pass
11	approximate entropy	1	0.06023	1.00	Pass
12	random excursions	8	0.37680	0.99	Pass
13	random excursions variant	18	0.36126	0.99	Pass
14	serial	2	0.30816	1.00	Pass
15	linear complexity	1	0.93195	0.99	Pass

[a]The results of multiple tests are averaged.

6. Conclusion

In this paper, we introduced a discrete memristive chaotic map generated by the combination of a quadratic discrete memristor with the sine function. To increase the complexity, we applied a chaotification method. Numerical analysis shows that the generated map has rich dynamical behaviors including more positive Lyapunov exponents and larger hyperchaotic range. As an application, we used the map cascaded with two seed maps to generate pseudo-random sequences. The NIST test results demonstrated it has good randomness and unpredictability. Next, we will focus on studying fractional-order discrete memristors and their applications.

Acknowledgement

Project supported by the National Natural Science Foundation of China (Grant Nos. 61901530, 62071496, and 62061008).

References

[1] Chua L 1971 *IEEE Transactions on Circuit Theory* **18** 507
[2] Chua L and Kang S 1976 *Proc. IEEE* **64** 209
[3] Strukov D B, Snider G S, Stewart D R and Williams R S 2008 *Nature* **453** 80
[4] Corinto F and Forti M 2017 *IEEE Transactions on Circuits and Systems I-Regular Papers* **64** 1540
[5] Valov I, Linn E, Tappertzhofen S, Schmelzer S, van den Hurk J, Lentz F and Waser R 2013 *Nat. Commun.* **4** 1771
[6] Zhao B, Xiao M and Zhou Y N 2019 *Nanotechnology* **30** 425202
[7] Wang Y, Ma J, Xu Y, Wu F and Zhou P 2017 *Int. J. Bifur. Chaos* **27** 1750030
[8] Kim H, Sah M, Yang C J, Cho S and Chua L 2012 *IEEE Transactions on Circuits and Systems I-Regular Papers* **59** 2422
[9] Zhang Y, Zhuang J S, Xia Y H, Bai Y Z, Cao J and Gu L F 2019 *Commun. Nonlinear Sci. Numer. Simul.* **77** 40
[10] Nagamani G, Rajan G and Zhu Q X 2020 *IEEE Transactions on Cybernetics* **50** 4281
[11] Li C, Hu M, Li Y N, Jiang H, Ge N, Montgomery E, Zhang J M, Song W h, Davila N, Graves C E, Li Z Y, Strachan J P, Lin P, Wang Z, Barnell M, Wu Q, Williams R S, Yang J J and Xia Q 2018 *Nat. Electron.* **1** 52
[12] Haj-Ali A, Ben-Hur R, Wald N, Ronen R and Kvatinsky S 2018 *IEEE Micro* **38** 13
[13] Ruan J Y, Sun K H, Mou J, He S B and Zhang L M 2018 *Eur. Phys. J. Plus* **133** 3
[14] Wang C H, Xia H and Zhou L 2017 *Int. J. Bifurc. Chaos* **27** 1750091
[15] Bao B C, Bao H, Wang N, Chen M and Xu Q 2017 *Chaos, Solitons & Fractals* **94** 102
[16] Wang G Y, Zang S C, Yuan F and Iu H H C 2017 *Chaos* **27** 013110
[17] Wang, G Y, Cui M Z, Cai B Z, Wang X Y and Hu T L 2015 *Mathematical Problems in Engineering* **2015** 561901
[18] Peng Y X, Sun K H and He S B 2020 *Chaos Solitons & Fractals* **137** 109873
[19] Peng Y X, He S B and Sun K H 2021 *AEU-International Journal of Electronics and Communications* **129** 153539
[20] He S B, Sun K H, Peng Y X and Wang L Y 2020 *AIP Advances* **10** 015332
[21] Zhu W Y, Pu Y F, Liu B, Yu B and Zhou J L 2022 *Chin. Phys. B* **31** 060204
[22] Bao B C, Li H, Wu H, Zhang X and Chen M 2020 *Electron. Lett.* **56** 769
[23] Lin H R, Wang C H, Hong Q H and Sun Y C 2020 *IEEE Transactions on Circuits and Systems II-Express Briefs* **67** 3472
[24] Fu L X, He S B, Wang H H and Sun K H 2021 *Acta Phys. Sin.* **71** 030501 (in Chinese)
[25] Zhou L, Wang C H, Zhang X and Yao W 2018 *Int. J. Bifur. Chaos* **28** 1850050
[26] Gu J C, Li C B, Chen Y D, Iu H H C and Lei T F 2020 *IEEE Access* **8** 12394
[27] Li C B, Wang R, Ma X, Jiang Y C and Liu Z H 2021 *Chin. Phys. B* **30** 120511
[28] Mohanty N, Dey R and Roy B 2020 *Eur. Phys. J. Special Top.* **229** 1231
[29] Zhang Y, Liu Z, Wu H, Chen S and Bao B 2019 *Chaos, Solitons and Fractals* **127** 354
[30] Pham V, Volos C and Fortuna L 2019 *Eur. Phys. J. Special Top.* **228** 1903
[31] Yang Y, Wang L D, Duan S K and Luo L 2021 *Optics and Laser Technology* **133** 106553
[32] Zhou Y C, Hua Z Y, Pun C M and Chen C 2015 *IEEE Transactions on Cybernetics* **45** 2001
[33] Bao B C, Rong K, Li H Z, Li K X, Hua Z Y and Zhang X 2021 *IEEE Transactions on Circuits and Systems II-Express Briefs* **68** 2992
[34] Hua Z Y, Zhou B H and Zhou Y C 2019 *IEEE Transactions on Industrial Electronics* **66** 1273
[35] Hua Z Y, Yi S, Zhou Y C, Li C Q and Wu Y 2018 *IEEE Transactions on Cybernetics* **48** 463
[36] Zheng Y G, Chen G R and Liu Z R 2003 *Int. J. Bifur. Chaos* **13** 3443
[37] Yuan F, Bai C J and Li Y X 2021 *Chin. Phys. B* **30** 120514
[38] Chua L 2014 *Semicond. Sci. Technol.* **29** 104001
[39] Adhikari S, Sah M, Kim H and Chua L 2013 *IEEE Transactions on Circuits & Systems I- Regular Papers* **60** 3008
[40] Bao H, Hua Z Y, Li H Z, Chen M and Bao B C 2021 *IEEE Transactions on Circuits and Systems I-Regular Papers* **68** 4534
[41] Hua Z Y, Zhou Y C and Bao B C 2019 *IEEE Transactions on Industrial Informatics* **16** 887
[42] Richman J S and Moorman J R 2000 *American Journal of Physiology-Heart and Circulatory Physiology* **278** H2039
[43] Han X T, Bi X G, Sun B, Ren L J and Xiong L 2022 *Front. Phys.* **10** 911144
[44] Chen C, Sun K H and He S B 2019 *Eur. Phys. J. Plus* **134** 410